

Numerical Boundary Layer Validation Technique using RAE M2155 Swept Wing

Hisham Mohsin[1], Simon A. Prince[1], Davide Di Pasquale[1]

[1]Cranfield University, Bedfordshire, MK43 0AL, United Kingdom

Abstract

In aerodynamics, generating high-quality data, whether numerical, experimental, or flight test, presents significant challenges. Achieving reliable solutions especially in Computational Fluid Dynamics (CFD), requires rigorous validation. One critical aspect of aerodynamic flow control is the importance of understanding the boundary layer (BL) behaviour, particularly on the suction side of a wing. Even when global parameters such as pressure and forces appear accurate, discrepancies in near wall flow results can still contribute to the error in computational results. This paper presents a validation study on the Royal Aeronautical Establishment (RAE) M2155 swept wing. Primarily using key experimental BL integral quantities to validate the numerical simulations. Tecplot® BL extraction macro was modified to improve integration accuracy by implementing Simpson rule to achieve the BL integral quantities. Comparisons between free air CFD simulations and modelling wind tunnel walls indicate that including the tunnel geometry improves agreement with experimental data. Among turbulence models tested, k-ω SST and GEKO provided the best match for BL characteristics. This work demonstrates that accurate BL extraction and validation are crucial for eventually designing flow control devices and defining appropriate numerical recipe to confidently capturing aerodynamic flow features.

Keywords: Transonic Aerodynamics, Boundary layer extraction, RANS CFD.

1. Introduction

The purpose of aerodynamic research in aeronautics is to achieve solutions that improve design efficiency, reduce costs, and minimize environmental impact. These goals are pursued through numerical, experimental, and flight test studies across multiple fidelity levels. Understanding the aerodynamic implications of wind tunnel testing and numerical results provides critical insight into the coherence of the underlying flow physics, particularly for complex phenomenon such as transonic buffet and shock boundary layer interactions.

Taking transonic buffet as an example, it is one of the most widely researched areas yet still one of the most complex flow physics to understand for three-dimensional airliner wings. Buffet is inherently highly unsteady due to oscillatory shock movements separating flow around it and producing secondary effects, buffeting (structural response to the aerodynamic buffet), which decreases passenger comfort and increases structural fatigue and limits aircraft flight envelope. Buffet onset can be delayed by implementing aerodynamic flow-control devices, including both passive and active systems that modify the boundary-layer behavior and local pressure distribution

Managing the complex shock-wave/boundary-layer interaction (SWBLI) is central to controlling buffet onset on transonic wings. Although various passive and active flow-control devices can target specific features of the SWBLI, their effectiveness is often limited to narrow operating regimes. Moreover, these devices may introduce significant integration challenges on existing airframes and can degrade performance at the aircraft's design point. An example of flow control which is using spanwise heterogeneous sinusoidal ridge type geometry roughness to address low frequency shock oscillations that alleviates structural fatigue but does not necessarily reduce separation bubbles [1], however the technology could be used to reduce separation with the penalty of not reducing shock oscillations. Vortex generators on the other hand, work by controlling the separation inside the boundary layer by energizing the boundary layer health and intern weakening the shock and moving it downstream. Overall point is that there are tradeoffs that need to be met with what is required to apply to a Technology Readiness Levels (TRL) 8 and above aircraft for commercial use.

To ensure that the relevant flow physics are accurately captured, significant emphasis is placed on validating analysis techniques, particularly computational methods, to guarantee the generation of high-fidelity, reliable aerodynamic data. The purpose of this paper is to validate the numerical approach for a broader study to effectively design flow control devices. The main area of validating the numerical approach is the BL extraction method using two postprocessing software Tecplot® and MATLAB®. Validation of the numerical methodology is performed using the RAE M2155 wing, a well-established experimental reference that provides high-quality boundary-layer profiles and associated integral quantities. This configuration is particularly suitable for addressing the questions posed in the following section, while also representing a realistic finite-wing geometry. Boundary-layer characteristics are emphasised because they fundamentally govern the viscous modification of the effective aerodynamic shape. Accurate prediction of boundary-layer development is essential for capturing shock location, shock strength, surface-pressure distributions, and the overall shock–boundary-layer interaction. In turn, these features directly influence aerodynamic forces and the fidelity of the simulated flow physics. The objective of this study is to identify the numerical approach, including the turbulence model and computational setup, that provides the closest agreement with the available experimental data. In addition, the study aims to assess and validate the accuracy of the boundary-layer (BL) extraction methodology. Two key research questions are addressed: (i) whether modelling the wind-tunnel test section is necessary to accurately reproduce the experimental results, or if a free-air computational domain is sufficient; and (ii) the extent to which the BL extraction method can reproduce experimentally measured boundary-layer characteristics. To investigate these questions, the RAE M2155 (‘Harrier’) wing was selected as the test case because of its three-dimensional swept-wing geometry and the availability of detailed experimental data suitable for replication in the commercial Computational Fluid Dynamics (CFD) solver ANSYS Fluent®. A sensitivity study was subsequently conducted to evaluate the influence of turbulence modelling and mesh resolution on the predicted aerodynamic and boundary-layer characteristics. Finally, a boundary-layer extraction macro implemented in Tecplot was employed and further modified to calculate integral boundary-layer parameters, enabling a detailed comparison between numerical predictions and experimental measurements. The contribution highlights the importance of minimising numerical assumptions to ensure that computational predictions remain consistent with the underlying physical phenomena and, where possible, are validated against experimental observations. Additionally, the study introduces a modified boundary-layer extraction methodology based on integral quantities, enabling the calculation of boundary-layer properties providing a more robust and versatile framework for boundary-layer analysis while maintaining consistency with established integral methods.

2. Methodology

2.1 Experimental Test Case Selection

The ‘Harrier’ wing, RAE Model 2155, was first introduced by M.C.P. Firmin and M.A. McDonald [2]. Their detailed experimental results were presented to further understand the flow around low-aspect ratio wings in the transonic regime close to the separation boundary. They tested their models over wide range of Mach numbers, from $\mathrm{M} = 0.6$ to $\mathrm{M} = 0.87$ at $\mathrm{Re_c} = 4.1 * 10^6$ acquiring surface pressure data over multiple chordwise locations along their respective spanwise locations from root to tip. The model was a half span wing mounted to the wall of the 2.4m x 1.8m Transonic Wind tunnel at Farnborough (UK). Solid walls were used in the test, and data corrections were applied for interference using P.R. Ashill and D.J. Weeks method for solid sidewalls [3]. Pressure measurements on the tunnel walls were used to quantify the magnitude of blockage and upwash in the vicinity of the model and to assess the limitations of applying free-air corrections, particularly at the higher subsonic Mach numbers. However, explicitly modelling the wind tunnel walls in CFD is often more appropriate when comparing with experimental data, as it allows wall induced confinement and interference effects to be captured. The use of CFD for boundary interference evaluation and interpretation of wind tunnel measurements is well established in the literature and has been shown to improve understanding of discrepancies between free air simulations and experimental results [4, 5]. In this case the displacement thickness was provided for the sidewalls and was 5mm. This allowed tunnel area to be smaller and the side walls to be slip conditions. The reduction in cross sectional area of

the working section was done by reducing the wall domain by 5mm each side (spanwise/Y direction and vertical/Z direction). For this study, CASE 1, 2 and 3 were selected as given in the reference for comparing not only pressure but also the BL data. Further information is provided in references [2, 6].

2.2 Numerical Setup

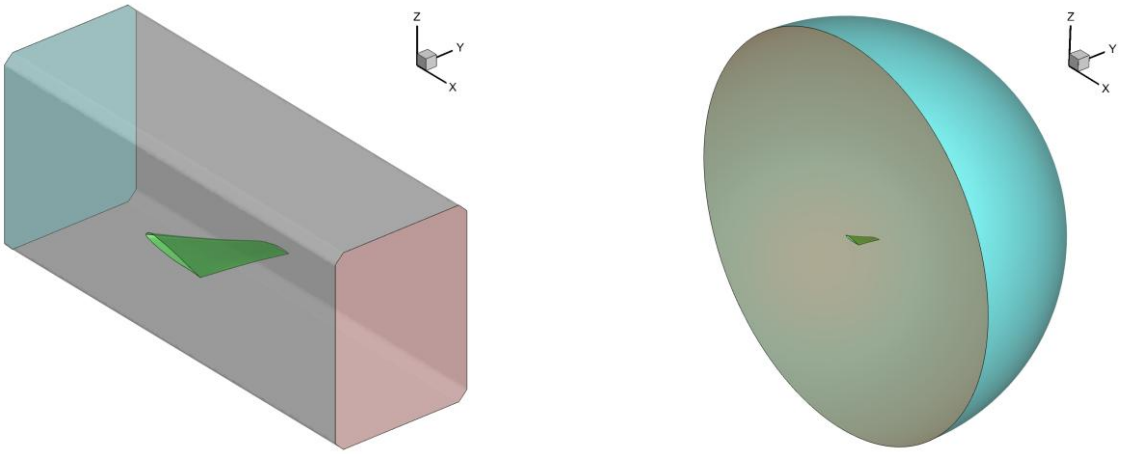
A CFD test matrix was generated which is shown in Table 1 to show what calculations were performed. ANSYS Fluent® was used for both mesh generation and simulating the flow on the grids generated. The domains used were as shown in Figure 1 (a) and (b). For Case 3 the upwash correction was applied to the twist as provided in the ESDU report [7] for the free air domain. The primary objective was to characterise the flow features and surface-pressure distribution and to assess their correspondence with the experimental measurements.

Table 1: Test matrix for all the 36 simulations conducted and completed.

M	Re	α [°]	Case	Turbulence model	Adapted Mesh	Flow Condition
0.744	4.1M	2.5	1	k – ϵ Realizable	NO	ATTACHED
0.744	4.1M	2.5	1	Spalart-Allmaras (SA)	NO	
0.744	4.1M	2.5	1	k – ω SST	NO	
0.744	4.1M	2.5	1	k – ω GEKO Csep 1	NO	
0.744	4.1M	2.5	1	k – ω GEKO Csep 2	NO	
0.744	4.1M	2.5	1	k – ω GEKO Csep 1.75	NO	
0.744	4.1M	2.5	1	k – ω Realizable	YES	
0.744	4.1M	2.5	1	Spalart-Allmaras (SA)	YES	
0.744	4.1M	2.5	1	k – ω SST	YES	
0.744	4.1M	2.5	1	k – ω GEKO Csep 1	YES	
0.744	4.1M	2.5	1	k – ω GEKO Csep 2	YES	
0.744	4.1M	2.5	1	k – ω GEKO Csep 1.75	YES	
0.806	4.1M	2.5	2	k – ϵ Realizable	NO	SLIGHT SEPARATION
0.806	4.1M	2.5	2	Spalart-Allmaras (SA)	NO	
0.806	4.1M	2.5	2	k – ω SST	NO	
0.806	4.1M	2.5	2	k – ω GEKO Csep 1	NO	
0.806	4.1M	2.5	2	k – ω GEKO Csep 2	NO	
0.806	4.1M	2.5	2	k – ω GEKO Csep 1.75	NO	
0.806	4.1M	2.5	2	k – ϵ Realizable	YES	
0.806	4.1M	2.5	2	Spalart-Allmaras (SA)	YES	
0.806	4.1M	2.5	2	k – ω SST	YES	
0.806	4.1M	2.5	2	k – ω GEKO Csep 1	YES	
0.806	4.1M	2.5	2	k – ω GEKO Csep 2	YES	
0.806	4.1M	2.5	2	k – ω GEKO Csep 1.75	YES	
0.843	4.1M	1.5	3	k – ϵ Realizable	NO	ATTACHED
0.843	4.1M	1.5	3	Spalart-Allmaras (SA)	NO	
0.843	4.1M	1.5	3	k-w SST	NO	
0.843	4.1M	1.5	3	k-w GEKO Csep 1	NO	
0.843	4.1M	1.5	3	k-w GEKO Csep 2	NO	
0.843	4.1M	1.5	3	k-w GEKO Csep 1.75	NO	
0.843	4.1M	1.5	3	k – ϵ Realizable	YES	
0.843	4.1M	1.5	3	Spalart-Allmaras (SA)	YES	
0.843	4.1M	1.5	3	k – ω SST	YES	
0.843	4.1M	1.5	3	k – ω GEKO Csep 1	YES	
0.843	4.1M	1.5	3	k – ω GEKO Csep 2	YES	
0.843	4.1M	1.5	3	k – ω GEKO Csep 1.75	YES	

For a numerical flow setup, ideal gas was selected with air as the fluid medium. The setting angle was changed for the model to the same geometric angle of attack with the tunnel walls modelled as slip walls. No transition trip was applied in the CFD setup. To get the correct Reynolds number of 4.1M, the pressure inlet and outlet were changed for each Case with the change of Mach number. Operating condition was set to 0Pa. The turbulence models selected for the study were, k-ω SST, k-ϵ Realizable and Spalart-Allmaras (SA) and the κ-ω GEKO [8] model. The GEKO model provides a framework that allows tuning of model coefficients to achieve comparable flow predictions. One of the key parameters is the Csep which can be varied between 0.7 and 2.5, inclusive. This parameter modifies the diffusion of the turbulence transport equations in boundary layers, thereby altering the distribution of turbulent kinetic energy and specific dissipation rate. As a result, it controls the eddy viscosity levels in the core of the boundary layer. Increasing Csep reduces eddy viscosity, decreasing turbulent mixing and momentum transfer toward the wall, which makes the boundary layer more sensitive to adverse

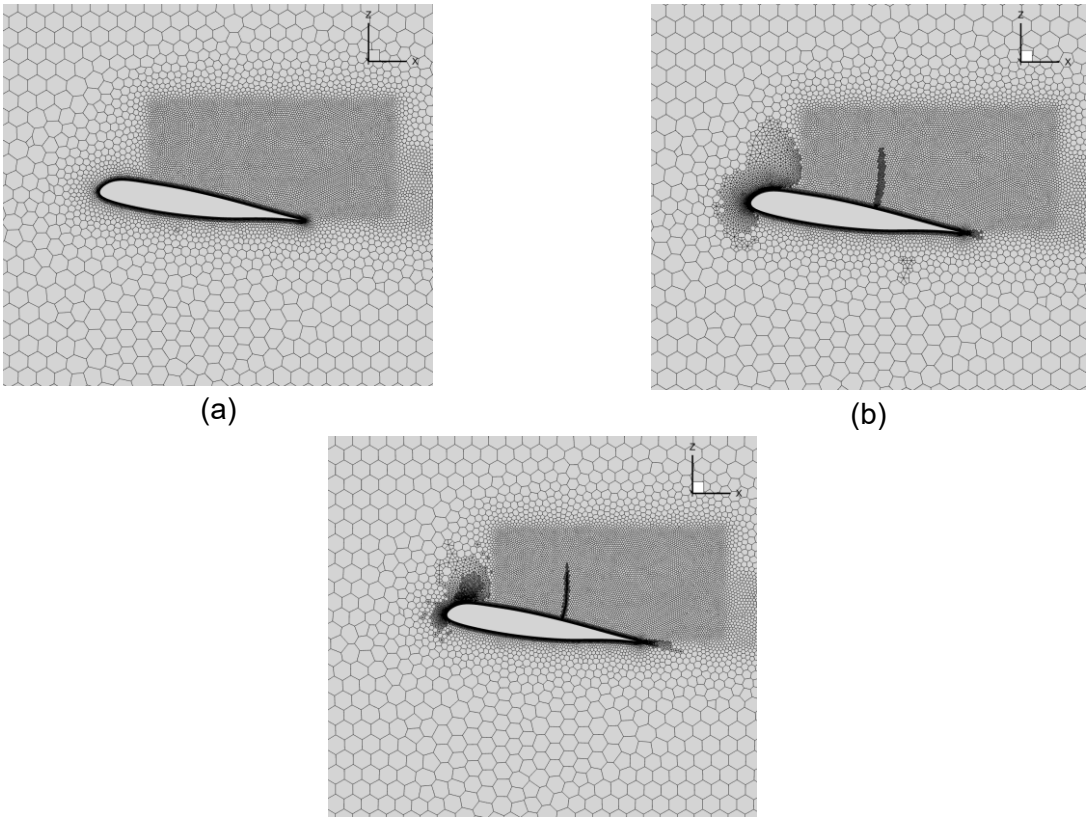
pressure gradients and leads to earlier separation. Similarly, lower values increase eddy viscosity and delay separation.



(a) (b)

Figure 1 - (a) Tunnel domain modelling side walls (as slip). (b) Domain for free air comparison.

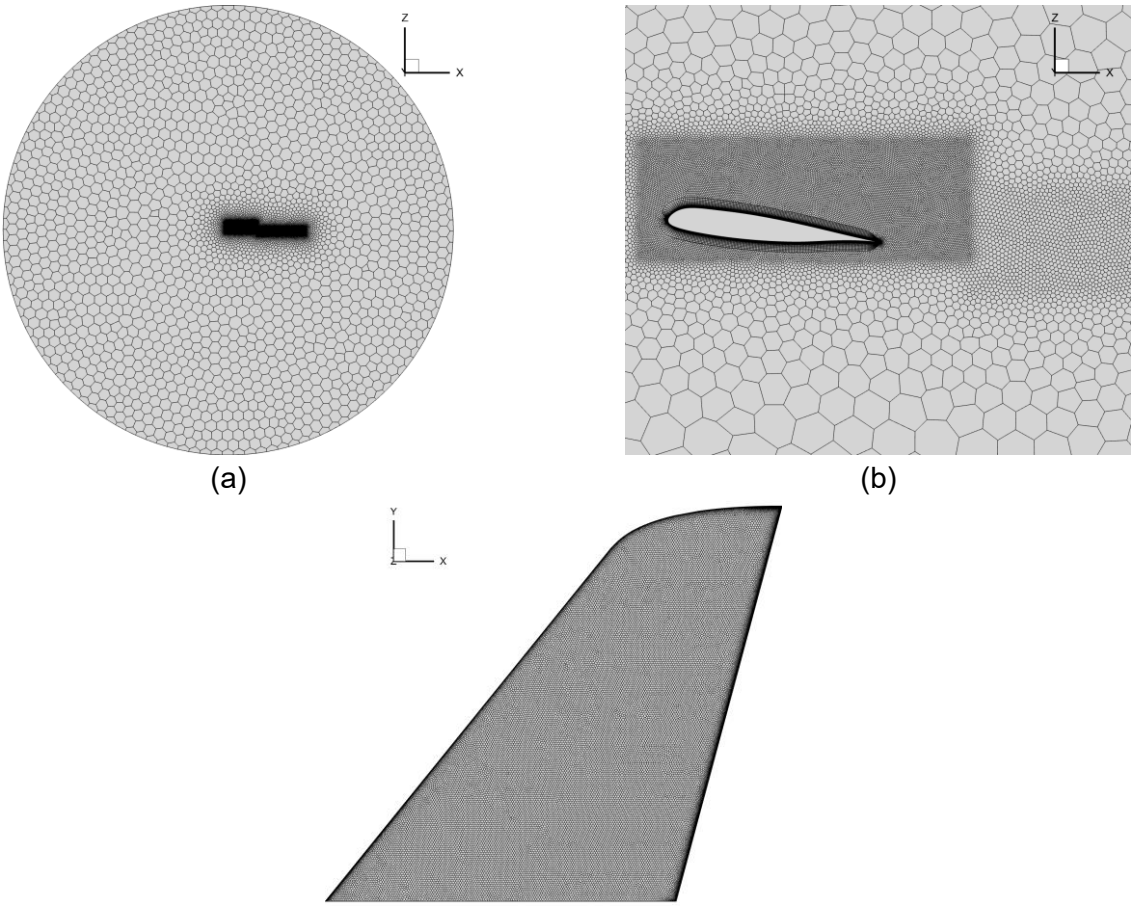
Poly-hexacore meshing strategy was applied to the fluid domains for the wind tunnel approach and free air approach. Images of these domains and respective refinements are shown in Figures 2 and 3. Figure 2 shows the mesh adaptation from the baseline mesh of 11M cells to 35M cells to 47M cells for the tunnel case. Overall pressure ratio '1-P/H' distribution (P is the static pressure and H is the total pressure) did not show much of a change between 35M to 47M, therefore the first refinement level was kept for further analysis. Regarding the free air flow case, the meshing strategy was kept similar to the tunnel CFD model (wake refinement flow refinement around model). The number of inflation layers was slightly higher in the free air but the growth layer and the first cell height was consistent. Figures 4 and 5 show the effect of turbulence models between $k-\omega\,SST$, SA, and $k-\epsilon\,Relaizable$ for $\eta = 40\%$ and $\eta = 80\%$. The overall comparison shows that the $k-\omega\,SST$ model performs well in capturing the surface pressures, especially the shock position and structure near to the tip.



(a) (b)

(c)

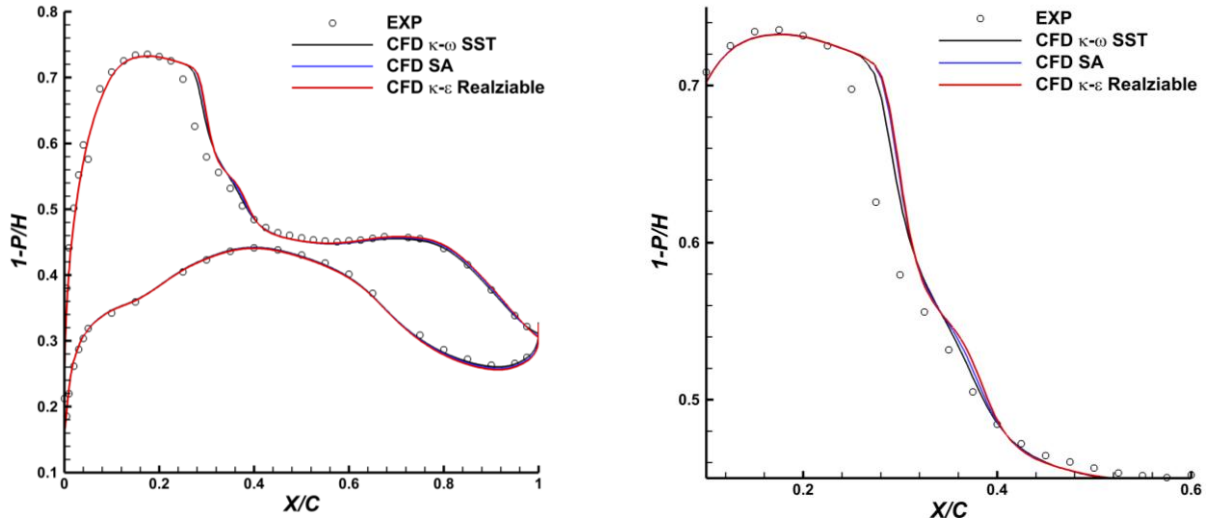
Figure 2 - Mesh refinement comparison around the RAE2822 Model (a) 11M Mesh, (b) 35M Mesh, and (c) 47M Cells.



(a) (b)

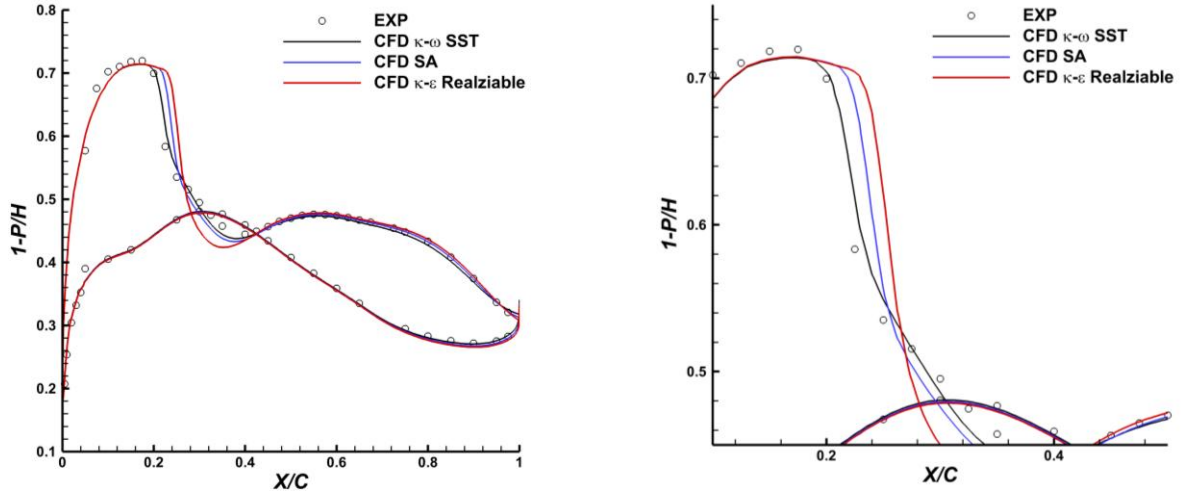
(c)

Figure 3 - (a) Side view grid for the free air case. (b) Zoomed side view around the airfoil. (c) Surface mesh for the M2115 wing.



(a) (b)

Figure 4 - (a) Case 2, $M = 0.806, Re_c = 4.1 * 10^6$ Turbulence model comparison at $\eta = 40\%$ (b) Zoomed in Picture around the shock location.



(a) (b)

Figure 5 - (a) Case 2, $M = 0.806, Re_c = 4.1 * 10^6$ Turbulence model comparison at $\eta = 80\%$ (b) Zoomed in Picture around the shock location.

2.3 Boundary layer extraction with modification

Post processing was conducted on Tecplot® and MATLAB® by attaining pressure distributions in the chordwise directions and the BL parameters. Initially, to extract BLs, the macro provided by Tecplot® was used. The description on how it was used is provided on the official website. The velocity profile extracted from Tecplot was imported to MATLAB to further analyze the results. The MATLAB script calculated the integral BL parameters and the boundary layer thickness using the 1/3 Simpsons rule. The equations used are provided in equations 1 to 4 and can be found in [9].

The boundary-layer thickness was calculated as the wall-normal distance Y at which the local BL velocity reached 99% of maximum velocity magnitude (of that profile). The displacement thickness and momentum thickness were calculated using the compressible integral quantities which considered the density ratio. A short internal code validation was done on the integration discretization method comparing the trapezoidal and 1/3 Simpsons rule. The result for both methods provided the same answers. It is important to state here that the point extracted normal to the lines were equally spaced and the resolution along the line was kept to 5000 points. The overall distance to extract depended on when the profiles reached freestream – inviscid shape. Therefore, the total distance extracted was usually double the boundary layer thickness. Additionally, the line can be plotted in fluent itself using the values from grid k unit normal (which represents the unit normality of the line on the surface) and the surface node location to extract, which is a manual process in itself.

$$\delta = [Y]_{\frac{U}{U_e}=0.99} \tag{1}$$

$$\delta^* = \int_0^{\delta} \left(1 - \frac{\rho * U}{\rho_e * U_e}\right) dy \tag{2}$$

$$\theta = \int_0^{\delta} \left(\frac{\rho * U}{\rho_e * U_e}\right) * \left(1 - \frac{U}{U_e}\right) dy \tag{3}$$

$$H = \frac{\delta^*}{\theta} \tag{4}$$

Due to the number of cases to simulate (shown in Table 1) and 28 measurement points over the upper surface of the wing, the MATLAB script and Tecplot® macro were combined into a single pytecplot script. This allowed to streamline the data extraction process. The main script of the BL extraction method was attained again from Tecplot® however, the script was modified to incorporate Simpson's integration, as implemented in MATLAB®, and was automated to process all 28 sampling locations by looping over the full set. Each location to extract boundary layers was matched to the closest node number of the fine surface mesh.

3. Results and Discussion

A short discussion on the comparison of the domain to tunnel is described in the following section which thereafter compares the pressure distributions across the span for each case and the relative turbulence models compared. The final section showcases most of the results on the boundary layer profiles and the evaluation of the integral quantities over the surface.

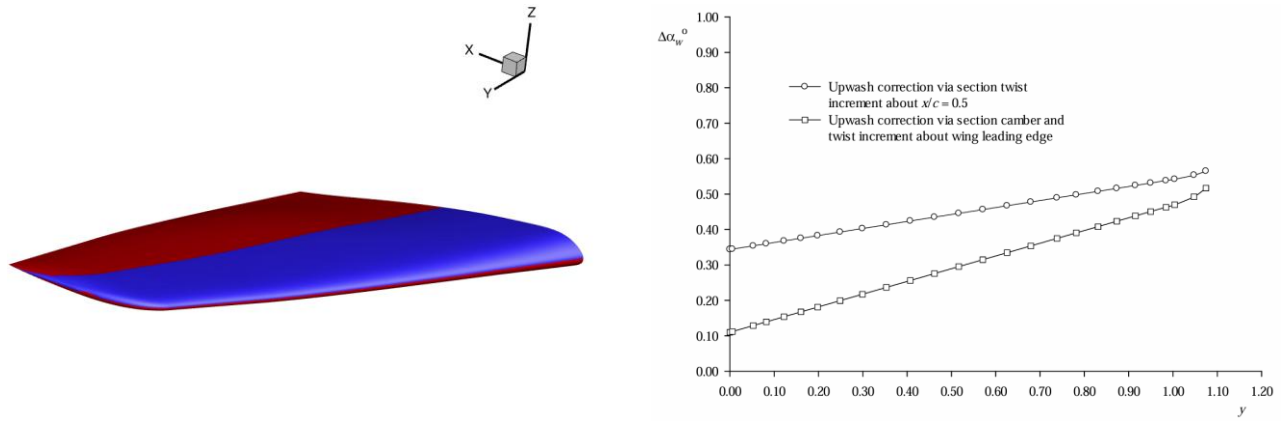
3.1 Effect of Domains

The effect of the flow domain was included as part of the validation study to assess whether Reynolds Averaged Navier Stokes (RANS) CFD can reproduce the flow conditions of the wind tunnel working section. This was investigated by modelling the tunnel walls and by comparison with a free-air configuration using a hemispherical computational domain. In addition, two versions of the M2115 wing were analysed: a baseline model corresponding to the experimental configuration with no upwash correction, and a modified model in which the wing twist was adjusted to account for tunnel upwash effects which are shown in Figure 6 (a). Simulations were conducted for Case 2 at $M = 0.806, \alpha = 2.5°$, and $Re = 4.1 * 10^6$.

The RAE M2155 model used for the free air calculations was corrected using the upwash-corrected twist distribution at $X/C = 50\%$ for each spanwise station, as defined in ESDU 13013 [7], and is shown in Figure 6 (b). Simulations within the tunnel domain were performed using both the uncorrected geometry, to replicate the experimental conditions, and the upwash-corrected geometry. It can be observed that maintaining consistency in the computational setup to align with the experimental configuration would provide the closest agreement with the experimental data [7]. This was shown in Figure 7 (a) and (b) where the pressure distributions obtained from both the free air and tunnel domains compared with experimental results. While overall differences are small, modelling the tunnel walls provides improved agreement with the experiment, particularly in terms of shock position, pressure rise gradient, and pressure recovery at spanwise locations of η = 40% and η = 80%. This is especially true if the model used in the wall tunnel CFD case is the one which has not had upwash corrections.

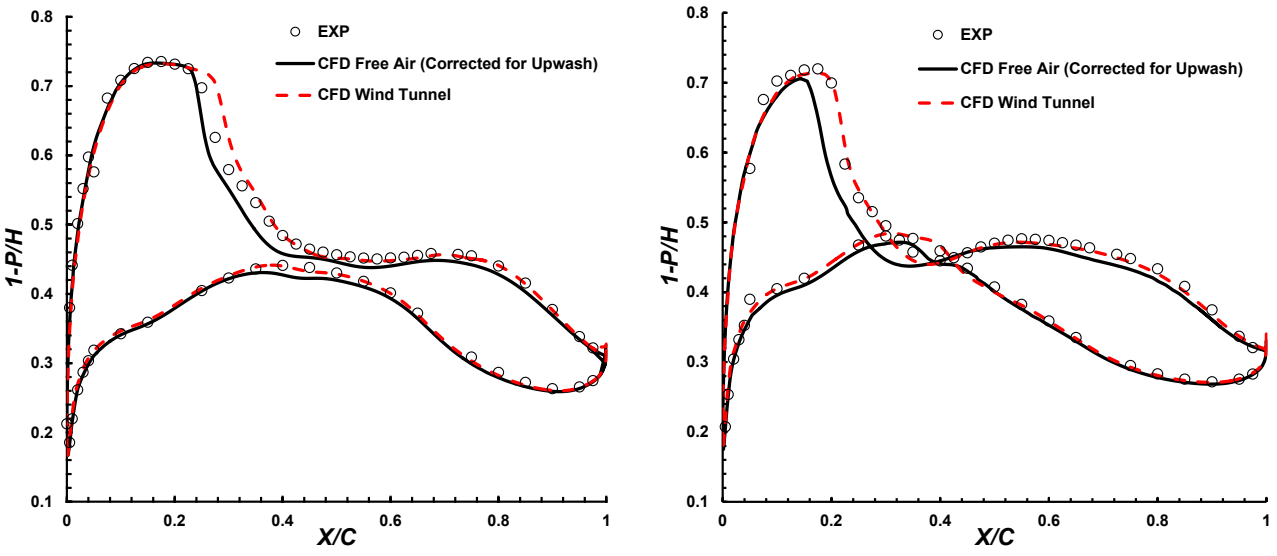
An interesting feature is observed in Figure 8, where the overall pressure distribution shape remains comparable to the experimental data; however, notable discrepancies appear particularly between $X/C \approx 30\ to\ 42\%$ and in the shock location, strength, and subsequent pressure recovery. The downstream shift of the shock in the case employing upwash-corrected geometry and is not attributed solely attribute to numerical blockage, but rather to an inconsistency between the upwash corrected geometry and the continued presence of wind-tunnel wall effects in the computational domain. The inconsistency is that upwash correction modifies the effective twist therefore modifying sectional loading to approximate free-air conditions. However, when tunnel walls are retained in the CFD simulation, lift interference and induced upwash are reintroduced (i.e., domain is smaller),

therefore, further altering the effective angle-of-attack distribution. This results in further change in circulation of the wing, that are observed as discrepancies on both the upper and lower surfaces, particularly in the near the mid chord region and shock position. Therefore, the domain selected to continue study was the M2155 model with no upwash correction with tunnel walls modelled just as what was shown in Figure 1 (a).



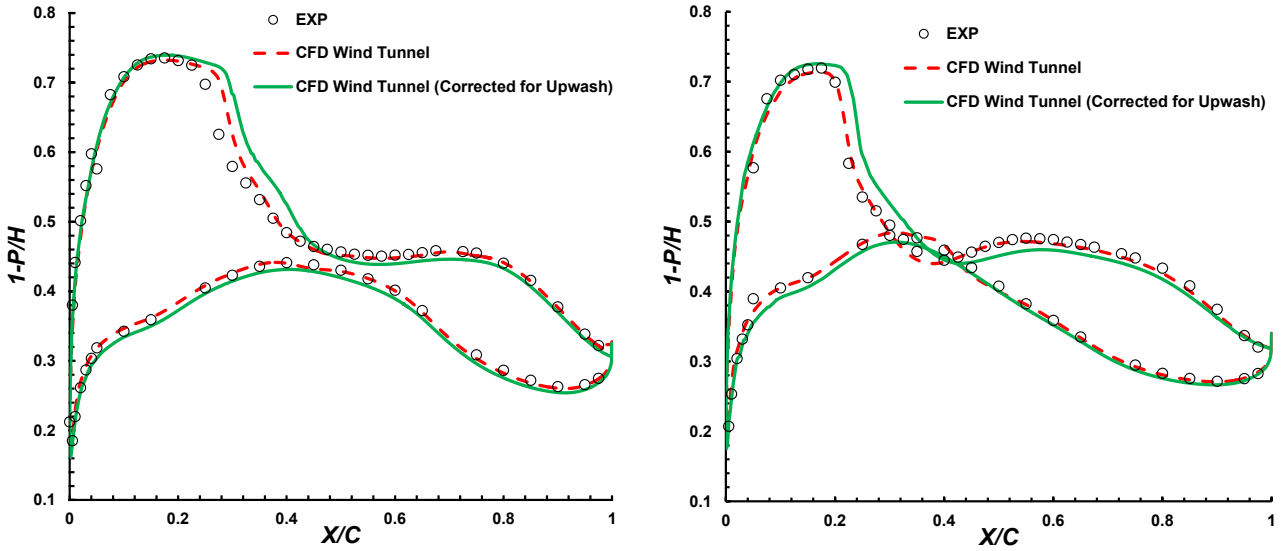
(a) (b)

Figure 6 – (a) M2155 with upwash corrections (blue) and without (red) upwash corrections, blue model twist is corrected along the X/C=50% (b) Twist distribution graph for the model taken from ESDU 13013 [7].



(a) (b)

Figure 7 – Pressure plot comparison for $M = 0.806, Re_c = 4.1 * 10^6$ comparing experimental tunnel case in RANS $k - \omega\ SST$ with free air that include upwash corrections (a) at $\eta = 40\%$ (b) at $\eta = 80\%$.



(a) (b)

Figure 8 - Pressure distribution comparison at $M = 0.806, Re_c = 4.1 * 10^6$ modelling tunnel walls with corrected for upwash model and no corrected upwash model for (a) at $\eta = 40\%$ (b) at $\eta = 80\%$. Both for $k - \omega\ SST$.

3.2 Results for Wind Tunnel Comparison

As mentioned previously, the model consisted of extracting 28 boundary layer profiles and their respective integral quantities over 36 simulations. Therefore, to limit the repetitive process of calculation and extraction, the pytecplot script was run over multiples times which output the velocity profiles with its perspective boundary layer thickness, displacement thickness, momentum thickness and the shape factor. The results presented in the figures below represent a subset of a much larger dataset, but they collectively illustrate a clear and consistent picture of the CFD validation outcomes.

The wind tunnel working section was modeled in CFD with Cases 1 to 3 compared to experiments in terms of BL and pressure plots. The upper surface was compared as that was the most critical area for future designs of flow control and studying SWBL effects. The results were compared across spanwise in the chordwise direction by the method described above.

Some of the results were shown in figures 9 to 11 mainly for two spanwise positions, inboard $\eta \sim 28\%$ and outboard $\eta = 78\%$ for Case 1, $M = 0.744, Re_c = 4.1 * 10^6$. These figures compare different turbulence models for the baseline grid and the effect they have on the boundary layer integral quantities normalised to the geometric mean chord, $\bar{C}$. The overall trend matches quite closely between the different turbulence models. The interesting feature is that the $\kappa - \epsilon$ Realizable slightly over predicts the BL thickness near the tip but has a consistent match with the experiment and other turbulence models near to the root. However, the overall trends are appropriately captured between the different models. Additionally, the shape factor towards the tip does not fully sit on the experimental results this implies that the ratio between the displacement thickness and momentum thickness underpredicts the momentum thickness from 20% to 80% of the chord. Furthermore, the figures showed similar trends between the turbulence models $\kappa - \omega$ SST and $\kappa - \omega$ GEKO. A detailed analysis was conducted over all the three test cases where the girds were adapted however only a few are shown here.

Grid adaptations in the regions of the shock and wake for the same turbulence models are compared to the unrefined cases to observe if the grid adaptation affects the result in a manner that reaches closer comparison to the experiment. These are shown for Case 2, $M = 0.806, Re_c = 4.1 * 10^6$ in Figures 12 to 14. The overall trend is consistent with the behavior observed in Case 1, with the additional observation that mesh adaptation did not increase the spread in the results; instead, it produced only a subtle modification to the solution. This subtle change increases the accuracy for the $\kappa - \omega$ SST model specifically seen in Figure 14 (a). Additionally, $\kappa - \epsilon$ Realizable moved away from the to the experiment in Figure 13 (b), near the trailing edge. However, to properly define what model captures the overall trend properly, the boundary layer profiles were also examined.

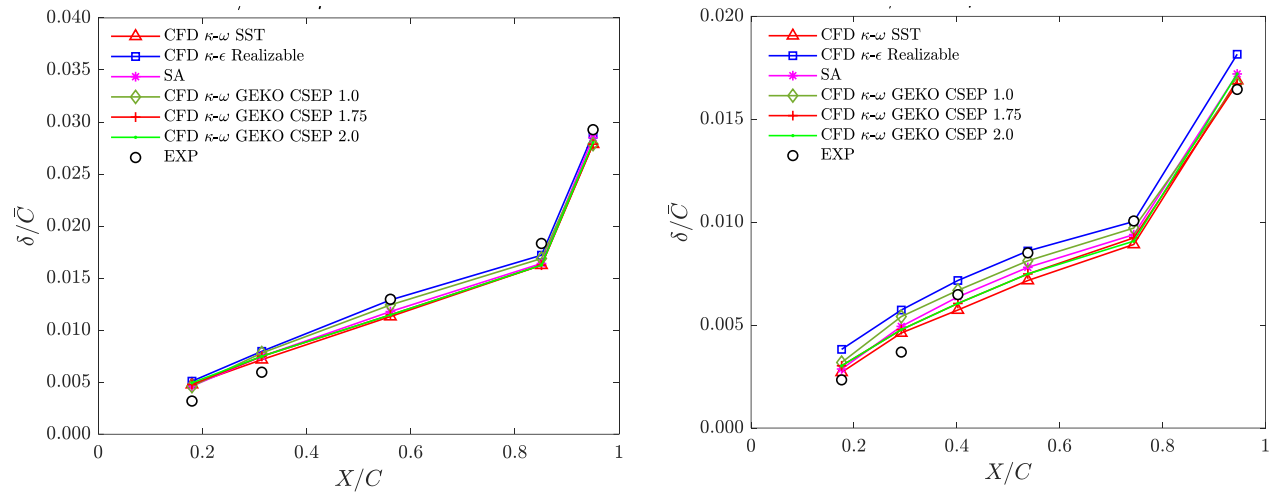


Figure 9 – Comparison of normalized δ values of different turbulrence models for $M = 0.744, Re_c = 4.1 * 10^6$ (a) $\eta = 27\%\ to\ 29.9\%$ (b) $\eta = 77\%\ to\ 79.8\%$.

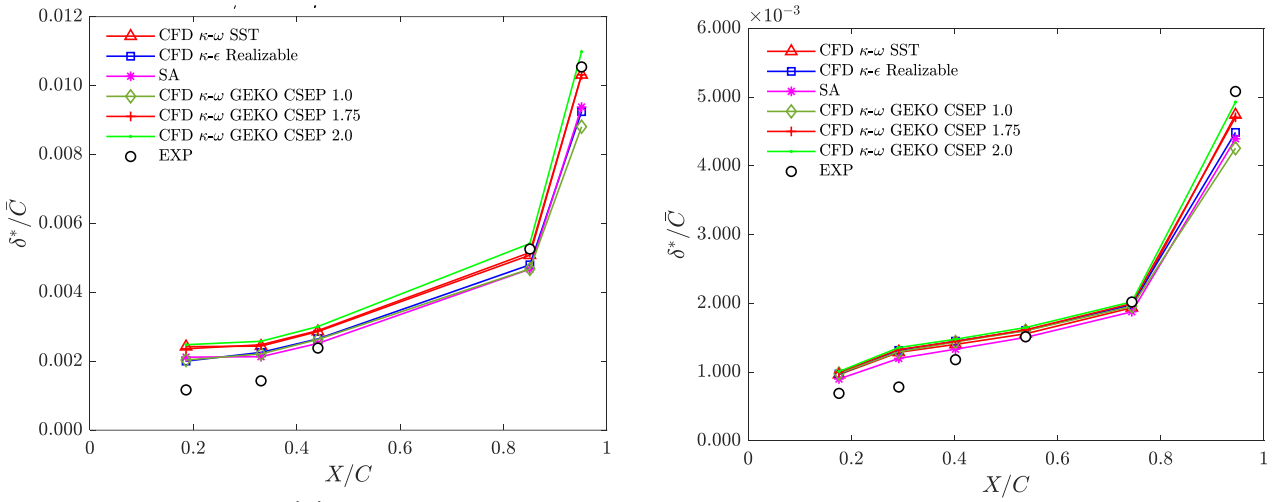


Figure 10 – Comparison of normalized δ^* values of different turbulrence models for $M = 0.744, Re_c = 4.1 * 10^6$ (a) $\eta = 27\%\ to\ 29.9\%$ (b) $\eta = 77\%\ to\ 79.8\%$.

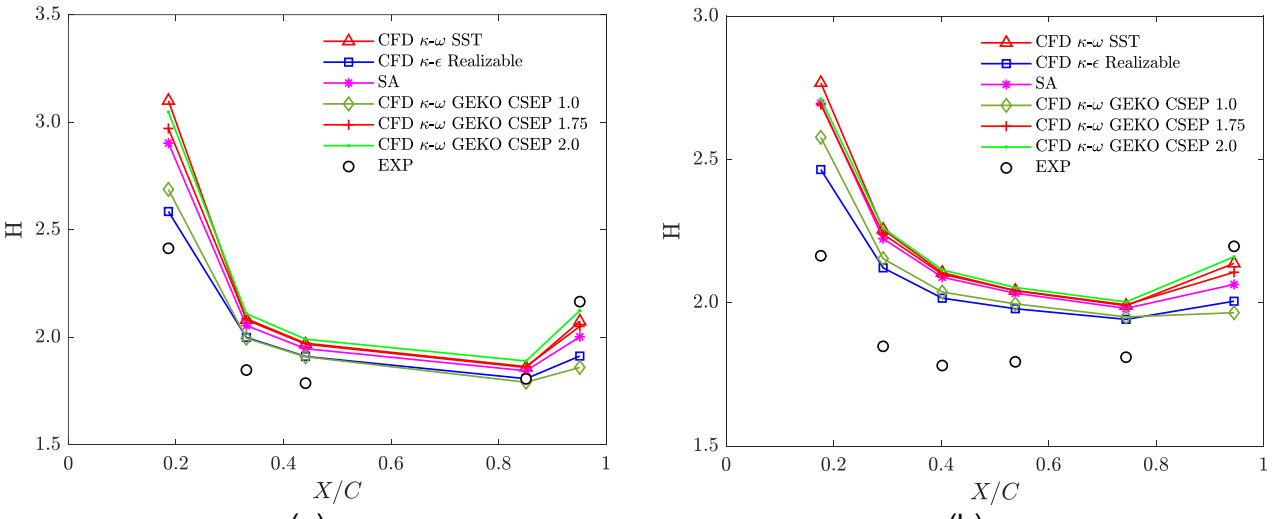
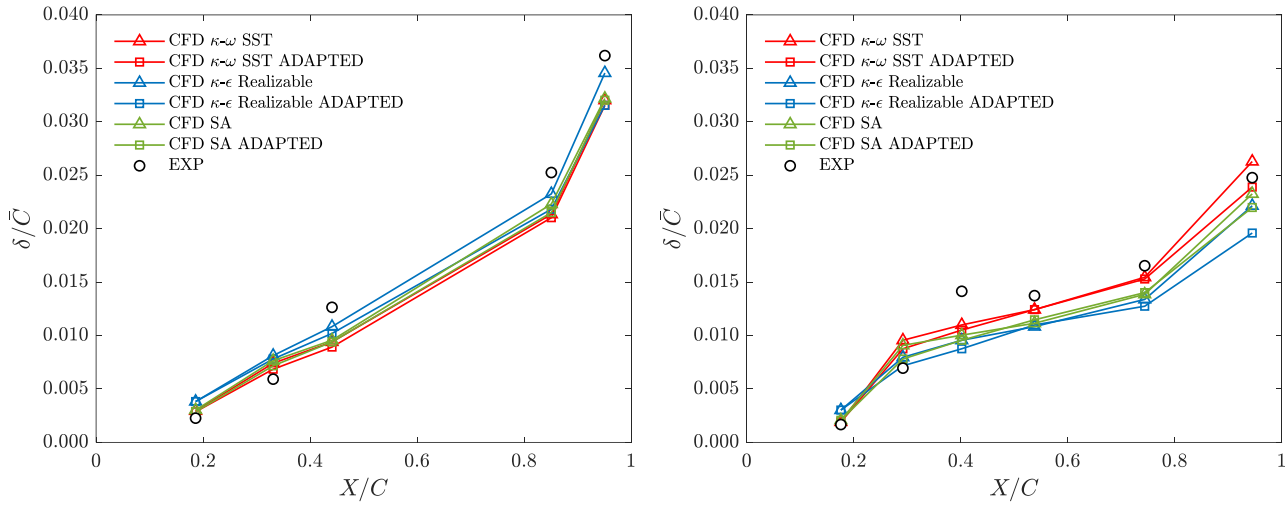
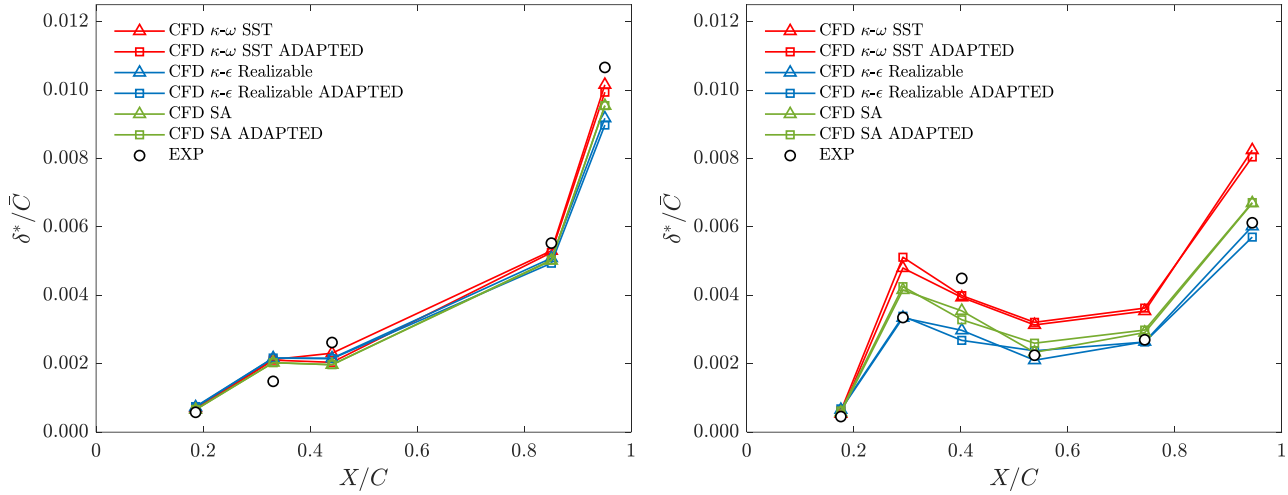


Figure 11 – Comparison of H values of different turbulrence models for $M = 0.744, Re_c = 4.1 * 10^6$ (a) $\eta = 27\%\ to\ 29.9\%$ (b) $\eta = 77\%\ to\ 79.8\%$.



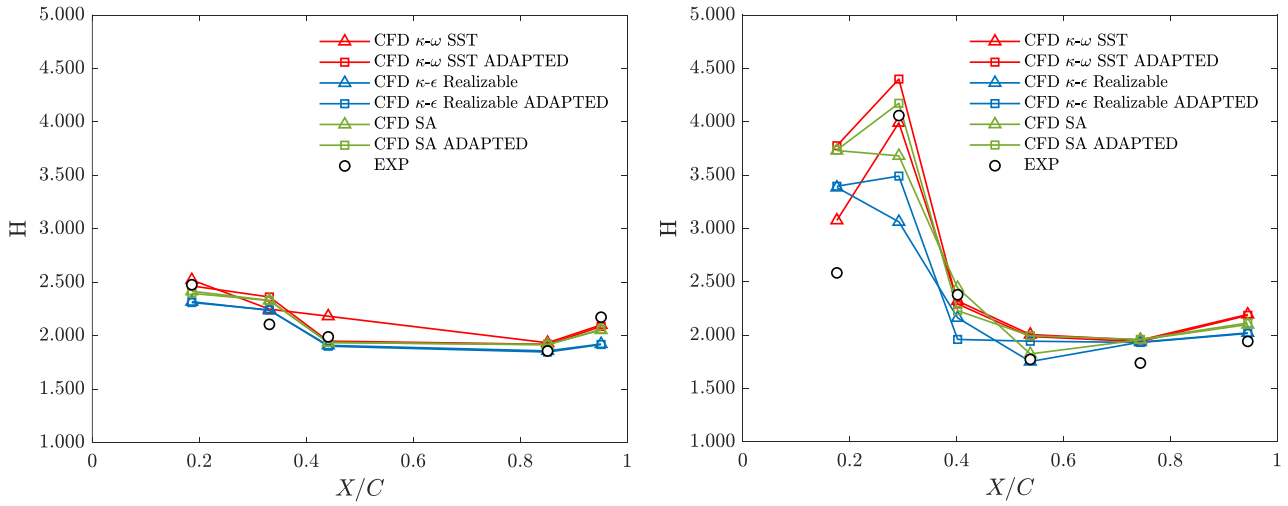
(a) (b)

Figure 12 – Comparison of normalized δ values of different turbulrence models between adapted and unadapted grids for $M = 0.806, Re_c = 4.1 * 10^6$ (a) $\eta = 27\%\ to\ 29.9\%$ (b) $\eta = 77\%\ to\ 79.8\%$



(a) (b)

Figure 13 – Comparison of normalized δ^* values of different turbulrence models between adapted and unadapted grids for $M = 0.806, Re_c = 4.1 * 10^6$ (a) $\eta = 27\%\ to\ 29.9\%$ (b) $\eta = 77\%\ to\ 79.8\%$



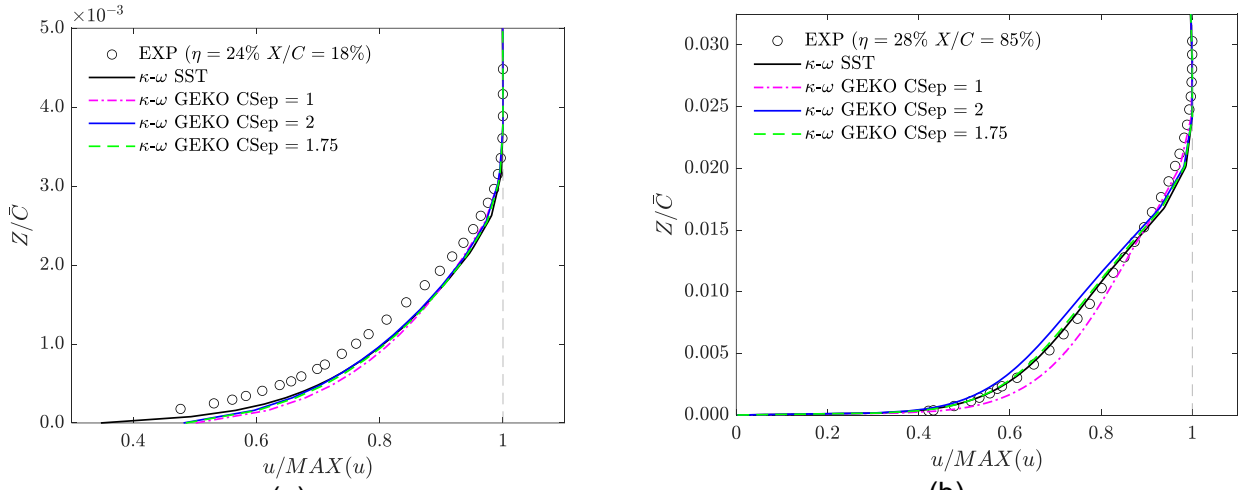
(a) (b)

Figure 14 – Comparison of H values of different turbulrence models between adapted and unadapted grids for $M = 0.806, Re_c = 4.1 * 10^6$ (a) $\eta = 27\%\ to\ 29.9\%$ (b) $\eta = 77\%\ to\ 79.8\%$.

Figures 15 and 16 present boundary layer velocity profiles for Case 2 and Case 1, respectively. Figure 15 compares the k − ω SST model with the k − ω GEKO model to assess the sensitivity of the boundary

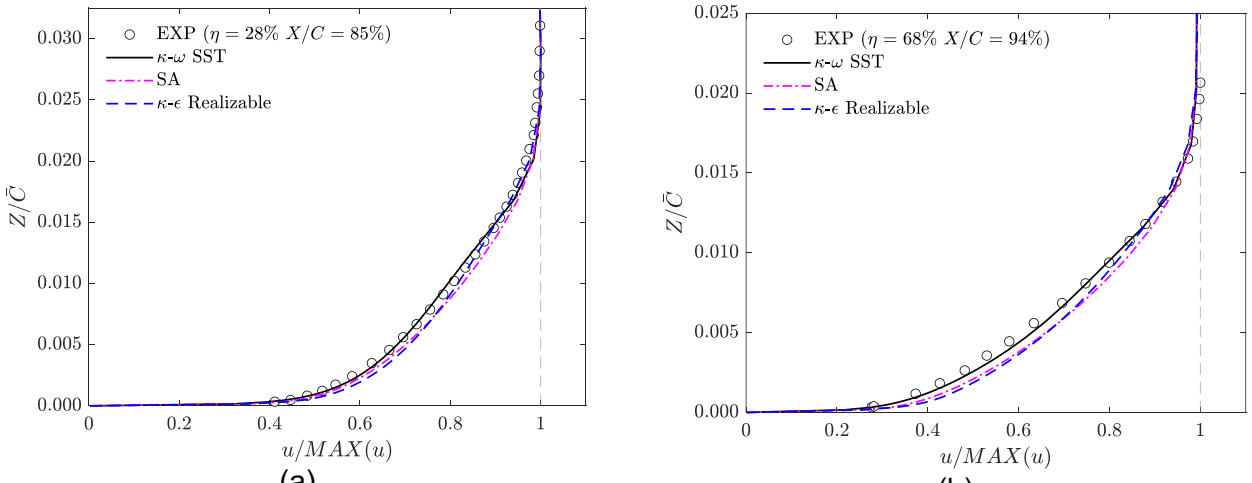
layer predictions to modified near wall parameters, specifically the Csep coefficient of the $\kappa - \omega$ GEKO model. The default GEKO and $k - \omega$ SST models show very similar boundary-layer profiles across the examined chordwise locations, indicating similar outcomes. A slight over-prediction of boundary-layer thickness is observed at X/C = 18%, which can be attributed to the developing turbulent boundary layer turbulent boundary layer downstream of the transition location in the experiment, whereas in these CFD calculations the boundary layer is turbulent from the leading edge. Based on these results, both the k–ω SST and GEKO models are considered suitable for the present analysis Varying this, Csep, coefficient produces only slight changes near the leading edge but leads to slightly fuller boundary layer profile downstream with a Csep coefficient of 1, particularly within the near wall sublayer. Increasing from 1.75 to 2.0 produces only minor changes however, the profile tends to look less full (more susceptible to adverse pressure gradients) at a value of 2. This is consistent with the intended role of Csep in the GEKO formulation for this swept wing case [8].

Figure 16 compares boundary layer profiles obtained using the $k - \omega$ SST, $k - \varepsilon$ Realizable, and SA models. Near the trailing edge, the $k - \omega$ SST model shows slightly improved agreement with the experimental profiles. However, the SA and $k - \varepsilon$ Realizable models also provide reasonable agreement over most of the chord which is observed in Figure 16 (a). Considering the boundary layer profiles, integral quantities and the pressure distributions, the $k - \omega$ SST and default GEKO models demonstrate the closest overall trade off to match the experiment. These models were therefore selected for further analysis. The SA model can also be identified as a viable alternative over the k–ε Realizable.



(a) (b)

Figure 15 – Comparison of computed and measured boundary layers, Case 2, $M = 0.806, Re_c = 4.1 * 10^6$ (a) near the leading edge (b) just upstream of the trailing edge.



(a) (b)

Figure 16 – Comparison of computed and measured boundary layers, Case 1, $M = 0.744, Re_c = 4.1 * 10^6$ (a) just upstream of the trailing edge (b) near the trailing edge.

4. Conclusions:

This work demonstrated that boundary layer extraction from RANS CFD provides trends that are in good agreement with experimental measurements for the cases examined. This validated the boundary layer extraction post processing method with the addition of calculating the momentum and displacement thicknesses using their integral equations. Although only a portion of the results are presented in the paper, the results highlight the importance of closely matching the experimental configuration in CFD simulations, particularly for high subsonic conditions where wind tunnel interference effects are non-negligible. Modelling the tunnel walls, together with appropriate boundary-layer representation showed to improve agreement with experiment, especially in regions influenced by shock development and pressure recovery. Among the turbulence models assessed, the k–ω SST model provided a good agreement for the different features that were being compared. Although, it is important to be stated, when comparing the boundary layer shape factor, the Spalart-Allmaras, and the default GEKO model did show a slightly better match. Therefore, these could be alternatively used for locally improved agreement in specific regions. Finally, the modified automated Tecplot® approach offers a robust tool for CFD post-processing and enhances confidence in numerical recipes for transonic flow studies.

5. Contact Author Email Address

Mail to: hisham.mohsin@cranfield.ac.uk;

6. Copyright Statement

The authors confirm that they, and/or their company or organization, hold copyright on all of the original material included in this paper. The authors also confirm that they have obtained permission, from the copyright holder of any third-party material included in this paper, to publish it as part of their paper. The authors confirm that they give permission, or have obtained permission from the copyright holder of this paper, for the publication and distribution of this paper as part of the ICAS proceedings or as individual off-prints from the proceedings.

7. References

[1] W. Wu, L. Laduarda, D. Modesti and S. Hickel, "Passive control of shock-wave/turbulent boundary-layer interaction via ridge-type roughness," Journal of Fluid Mechanics, vol. 1029, p. 33, 2026.

[2] M. Firmin and M. McDonald, "Measurments of the flow over a low aspect-ratio wing in the Mach number range 0.6 to 0.87 for the purpose of validation of computational methods," DRA, Farnborough, 1992.

[3] P. Ashill and D. Weeks, "A method for determining wall-interference corrections in solid-wall tunnels from measurements of static pressure at the walls.," AGARD CP 335 - paper 1, 1982.

[4] C. Britcher and D. Landman, "The role of computational fluid dynamics in aerodynamics research," in Wind Tunnel Test Techniques: : Design and Use at Low and High Speeds with Statistical Engineering Applications, Academic Press, 2023, p. 626.

[5] AGARD-AG-336, "Wind Tunnel Wall Corrections," AGARD, Neuilly-sur-Seine, 1998.

[6] AGARD-AR-303 Volume II, "A Selection of Experimental Test Cases for the Validation of CFD Codes," AGARD, 1994.

[7] ESDU 13013, "Viscous full-potential (VFP) method for three-dimensional wings and wing-body combinations Part 1: Validation of results with experiment and comparisons with other methods," ESDU, 2014.

[8] Menter and Matyushenko, "Generalized k−ω (GEKO) Two-Equation Turbulence Model," AIAA Journal, vol. 63, no. 11, pp. 4498-5027, 2025.

[9] D. Whitfield, "Integral solution of compressible turbulent boundary layers using improved velocity profiles," Arnold Engineering Development Center/DOTR, Tennessee, 1978.